

Silver nanoparticle array structures that produce remarkably narrow plasmon lineshapes

Shengli Zou, Nicolas Janel,^{a)} and George C. Schatz

Department of Chemistry, Northwestern University, Evanston, Illinois 60208-3113

(Received 19 November 2003; accepted 21 April 2004)

Using electrodynamics calculations, we have discovered one dimensional array structures built from spherical silver nanoparticles that produce remarkably narrow (\sim meV or less) plasmon resonance spectra upon irradiation with light that is polarized perpendicular to the array axis. The narrow lines require a minimum particle radius of about 30 nm to achieve. Variations of the plasmon resonance wavelength, extinction efficiency and width with particle size, array structure, interparticle distance and polarization direction are examined, and conditions which lead to the smallest widths are demonstrated. A simple analytical expression valid for infinite lattices shows that the sharp resonance arises from cancellation between the single particle width and the imaginary part of the radiative dipolar interaction. © 2004 American Institute of Physics. [DOI: 10.1063/1.1760740]

The development of noble metal nanoparticle-based optical sensors is a very active area of nanoscience research.^{1–6} Numerous experiments show that the spectra of nanoparticle arrays are influenced by particle shape and size,^{7–9} the interactions between particles^{10–13} and the polarization of the incident light.^{14,15} Several theoretical studies have been carried out to provide a general understanding of the electrodynamics of nanoparticle arrays.^{16–19} In many cases, silver nanoparticle arrays show narrow plasmon resonance peaks in their extinction spectra, and as a result these structures are useful in chem/biosensor^{1,20–22} applications where the shift in plasmon wavelength upon analyte binding to the particle provides the sensing transduction mechanism.

In a previous theoretical study of the extinction spectra of one and two dimensional arrays of silver nanoparticles with radius 30 nm,¹⁷ the wavelength and width of the plasmon resonance that is produced by dipole coupling between the particles was successfully used to model recent experiments.²² Narrow resonances were found when the particle spacing was taken to be close to the plasmon wavelength, and both analytical theory which qualitatively explains the results,¹⁷ and numerical methods which quantitatively explain the results¹⁸ were developed. However the experiments did not consider array spacings that were predicted to give the narrowest plasmon lineshapes, and all the experiments considered two dimensional arrays with the polarization vector parallel to the plane of the array. In this paper, we describe an alternative array configuration that leads to much narrower plasmon resonances for large enough particles. This work is related to an earlier study by Markel,²³ who considered infinite one dimensional (1D) arrays in the quasistatic approximation, however here we have used a more general theory to show that finite 1D arrays with more than 50 particles produce remarkably narrow resonances if the particles are large enough. We also show that both the absorption and scattering lineshapes are narrow. Re-

lated behavior is found for two dimensional (2D) arrays but always with broader lineshapes. The desired array structures should be amenable to fabrication with lithography methods, so the structures we describe could have important consequences for chem/bio detection.

We use the coupled dipole (CD) method, for both finite and infinite lattices, to determine extinction, absorption and scattering spectra of 1D and 2D arrays of spherical particles. As a check, we have also performed exact T-matrix calculations (converged multipole expansions) for some of the structures, and the sharp resonance lineshapes that we present later are identical to the CD results so only the latter are presented.

The CD method is well known,²⁴ so here we give a very brief description. Consider an array of N particles whose positions and polarizabilities are denoted \mathbf{r}_i and α_i . The induced dipole \mathbf{P}_i in each particle in the presence of an applied plane wave field is $\mathbf{P}_i = \alpha_i \mathbf{E}_{\text{loc},i}$ ($i = 1, 2, \dots, N$), where the local field $\mathbf{E}_{\text{loc},i}$ is the sum of the incident and retarded fields of the other $N - 1$ dipoles. For a given wavelength λ , this field is

$$\mathbf{E}_{\text{loc},i} = \mathbf{E}_{\text{inc},i} + \mathbf{E}_{\text{dipole},i} = \mathbf{E}_0 \exp(i\mathbf{k} \cdot \mathbf{r}_i) - \sum_{\substack{j=1 \\ j \neq i}}^N A_{ij} \cdot \mathbf{P}_j, \\ i = 1, 2, \dots, N, \quad (1)$$

where E_0 and $k = 2\pi/\lambda$ are the amplitude and wave vector of the incident wave, respectively. The dipole interaction matrix A is expressed as

$$A_{ij} \cdot \mathbf{P}_j = k^2 e^{ikr_{ij}} \frac{\mathbf{r}_{ij} \times (\mathbf{r}_{ij} \times \mathbf{P}_j)}{r_{ij}^3} \\ + e^{ikr_{ij}} (1 - ikr_{ij}) \frac{[r_{ij}^2 \mathbf{P}_j - 3\mathbf{r}_{ij}(\mathbf{r}_{ij} \cdot \mathbf{P}_j)]}{r_{ij}^5} \\ (i = 1, 2, \dots, N, \quad j = 1, 2, \dots, N, \quad j \neq i), \quad (2)$$

^{a)}Present address: Ecole Supérieure d'Optique, Orsay, France.

where \mathbf{r}_{ij} is the vector from dipole i to dipole j . The polarization vectors are obtained by solving $3N$ linear equations of the form

$$\mathbf{A}'\mathbf{P}=\mathbf{E}, \quad (3)$$

where the off diagonal elements of the matrix, A'_{ij} , are the same as A_{ij} , and the diagonal elements of the matrix, A'_{ii} , are α_i^{-1} . After obtaining the polarization vectors, we can calculate the extinction cross section using:

$$C_{\text{ext}} = \frac{4\pi k}{|E_0|^2} \sum_{j=1}^N \text{Im}(\mathbf{E}_{\text{inc},j}^* \cdot \mathbf{P}_j). \quad (4)$$

In the case of an infinite array of particles, it is possible to generate an analytical solution to (3) for the case where the wave vector is perpendicular to the array axis (or plane) by assuming that the induced polarization in each array element is the same. This leads to the following expression for the polarization of each particle:

$$P = \frac{\alpha_s E_o}{1 - \alpha_s S} \quad \text{and} \quad C_{\text{ext}} = 4\pi N k \text{Im}(P/E_o), \quad (5)$$

where S is the retarded dipole sum

$$S = \sum_{j \neq i} \left[\frac{(1 - ikr_{ij})(3 \cos^2 \theta_{ij} - 1)e^{ikr_{ij}}}{r_{ij}^3} + \frac{k^2 \sin^2 \theta_{ij} e^{ikr_{ij}}}{r_{ij}} \right], \quad (6)$$

where θ_{ij} is the angle between r_{ij} and the polarization direction. Markel²³ has given analytical expressions for the dipole sums for 1D arrays, but it is not difficult to evaluate this numerically for 1D or 2D arrays.

Equation (5) provides a simple way to understand the effect of the coupling between the particles on the plasmon resonance lineshape. For small spherical particles close to resonance, the polarizability α_s is approximately $-A/(\omega - \omega_p + i\gamma)$, where A is a constant (which as demonstrated later is a positive real number for small particles), ω_p is the surface plasmon frequency for the isolated particle and γ is its half-width (note this is half the Drude width). If this is substituted into Eq. (5) we find

$$P = \frac{-AE_o}{\omega - \omega_p + i\gamma + AS} = \frac{-AE_o}{\omega - \{\omega_p - \text{Re}(AS)\} + i\{\gamma + \text{Im}(AS)\}}, \quad (7)$$

which means that the real part of AS (which if A is real, means the real part of S) determines the red or blue shift of the plasmon resonance frequency and the imaginary part determines the change in the width. In our earlier study^{17,22} we showed that for polarization parallel to the array, the real part of AS is typically positive when the particles are closer together than 100 nm, and this leads to red shifts in the spectra as the particle spacing decreases, while for larger separations (close to half a wavelength) the real part of AS is typically negative and blue shifts occur. The plasmon width can either increase or decrease with particle separation depending on

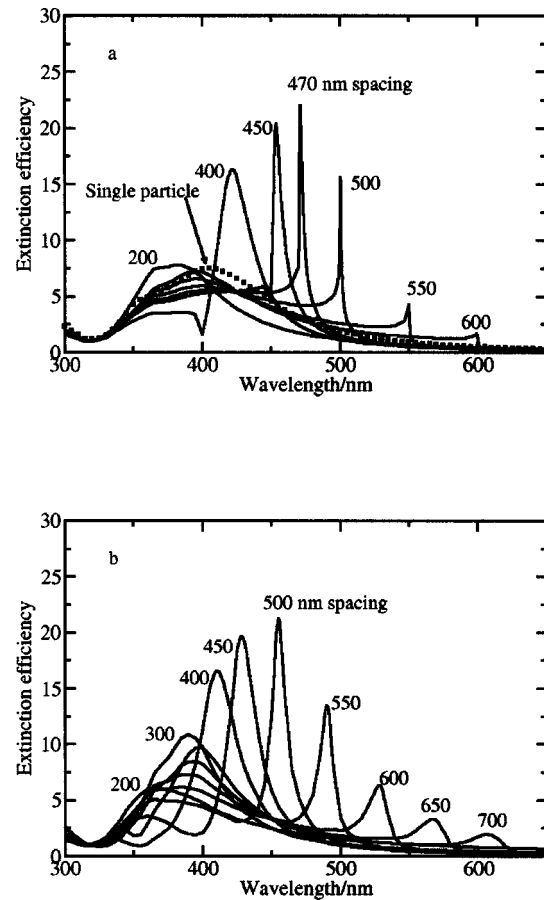


FIG. 1. Extinction spectra of 50 nm silver nanoparticles in (a) a one-dimensional chain of 400 particles, and (b) a two-dimensional hexagonal array of 400 particles. In the chain, the polarization vector and wave vector are both perpendicular to the chain. In the array, the wave vector is perpendicular to the plane and the polarization vector is in the plane.

values of the interparticle distance relative to the wavelength. Interestingly, we find that array structures exist where the width factor in Eq. (7), $\gamma + \text{Im}(AS)$, vanishes! [Of course deviations from the Lorentzian form in (7) can still lead to a finite width.] Such structures involve large particles (large value of A), and they occur when the radiative term in S (that varies as $1/r_{ij}$) dominates the dipole sum. The largest effect occurs for 1D arrays. In this case one should take the polarization perpendicular to the array axis [i.e., $\theta_{ij} = \pi/2$ in Eq. (6)] as this leads to the largest $1/r_{ij}$ contribution. This occurs when the plasmon wavelength is slightly greater than the array spacing, which means that the optical diffraction (photonic) mode associated with a perfectly periodic lattice couples to the plasmon mode of each particle to produce a combined mode with a remarkably sharp extinction profile.

We begin by considering finite length arrays in 1D and 2D and considering silver particles whose radii are 50 nm. The dielectric constants for the coupled dipole calculations are from Palik,²⁵ and the sphere polarizabilities are derived²⁶ from the a_1 term of Mie theory (i.e., not quasistatic). In both 1D and 2D arrays we take the wave vector perpendicular to the array axis or array plane, and in 1D we also take the polarization vector perpendicular to the axis. Figure 1 presents results (plotted as extinction efficiency, where effi-

ciency is the ratio of extinction cross section to geometrical area of the array) for different interparticle distances in the 200–700 nm range, for an array containing 400 particles, with Fig. 1(a) considering a 1D chain and Fig. 1(b) a 2D hexagonal array. The isolated particle spectrum is included for reference in Fig. 1(a). Figure 1(a) shows a dramatic narrowing and red shifting of the plasmon lineshape as particle separation is increased. The intensity peaks at a spacing of 470 nm, with a peak wavelength of 471.4 nm and a width (here ignoring the broad base of each peak in defining the width) of 3.5 nm (20 meV). The plasmon width narrows when we further increase the spacing, becoming 1.5 nm (7 meV) when the spacing is 500 nm, however the plasmon intensity is also reduced. Figure 1(a) refers to a wave vector that is perpendicular to the chain axis, but we have also done calculations for the parallel case, and we also find narrow plasmon resonances, but not as narrow as for the perpendicular wave vectors. However narrow resonances are only found for polarization perpendicular to the array axis. In the general case of arbitrary polarization direction and arbitrary wave vector direction, the sharp structures in Fig. 1(a) would still be a component of the lineshape. We have also studied the effect of random fluctuations in the array spacing, and we find that sharp lines are still present, although with diminished amplitude, when the particle location varies by as much as 50% of the lattice spacing. These points will be examined in detail in a future paper.²⁷

Figure 1(b) shows that for a 2D array, the variation in the plasmon peak with increasing particle separation is very similar to that in the 1D chains, but the plasmon is always broader. For example, there is a peak at 455 nm when the separation is 500 nm with a width of 14 nm (84 meV). Figure 1(b) refers to polarization parallel to the plane and wave vector perpendicular to the plane. Other choices of wave vector and polarization give broader lineshapes for a given spacing.

Now let us consider one dimensional arrays based on particles with radii 30 and 100 nm. Results analogous to those in Fig. 1(a) for arrays of 400 particles are presented in Fig. 2. For the 100 nm particles [Fig. 2(a)], we see behavior analogous to Fig. 1(a), but the most intense plasmon peak occurs at 802.0 nm for 800 nm spacing, and the plasmon width is 3.5 nm (7 meV). Narrower peaks are again found for larger separations; for example the width is 2.7 nm (5 meV) for a spacing of 840 nm. The results in Figs. 1(a) and 2(a) show that we are able to generate narrow plasmon peaks over the whole visible range by changing particle size and interparticle distance. In addition, we see that the minimum width for the larger particle size is about the same as that for the smaller one. This is to be contrasted with the isolated particle widths, which are much larger for the larger particles due to radiative damping effects. Also, note that intense plasmon resonances are only obtained for wavelengths that fall within the general envelope of the isolated particle lineshape.

In previous work by Zhao *et al.*¹⁷ the extinction spectrum of a 1D silver nanoparticle array with 30 nm particles and perpendicular polarization was briefly considered. They found that the plasmon narrowed when the interparticle distance was taken to be larger than 180 nm; however the larg-

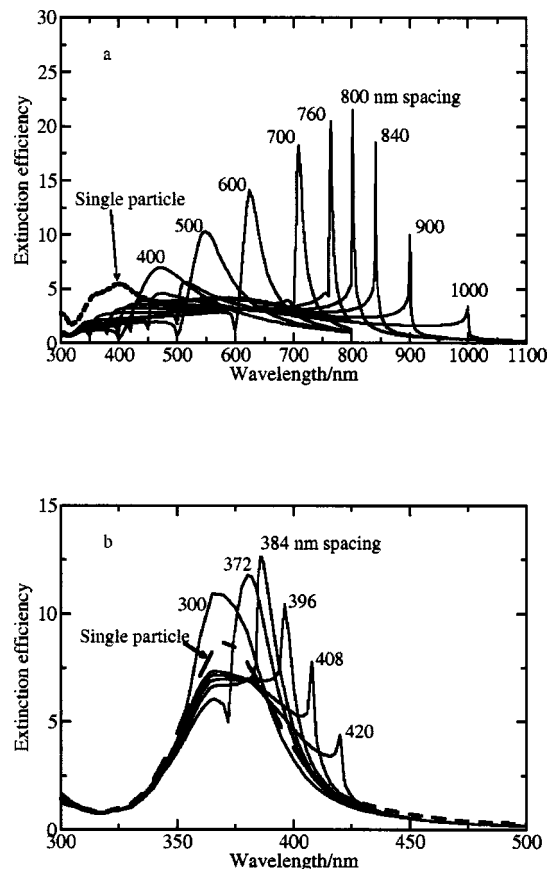


FIG. 2. Extinction spectra of one dimensional chains analogous to those in Fig. 1(a) for particles whose radii are (a) 100 nm and (b) 30 nm.

est spacing considered was 300 nm so sharp resonances analogous to those in Figs. 1(a) and 2(a) were not observed. Figure 2(b) shows results for 30 nm particles that have been extended to a spacing of over 400 nm. Here we again see sharp peaks analogous to Fig. 1(a), but the peaks are broader and less pronounced. When the spacing is 384 nm, the plasmon wavelength is 386 nm and the width is over 15 nm (125 meV). We also studied particles with a 20 nm radius and did not find sharp peaks appearing for any separation.

To further characterize the narrow plasmon peaks, we have calculated scattering and absorption efficiencies for 50 nm particles, analogous to the extinction spectra that were presented in Fig. 1(a). The results are shown in Figs. 3(a) (scattering) and 3(b) (absorption). By comparing Figs. 3(a) and 3(b) we find that scattering efficiencies are typically about twice as large as absorption. This ratio increases from 1.8 for an interparticle spacing of 200 nm to 2.1 for a spacing of 470 nm (the wavelength of peak extinction), and to 3.5 for a spacing of 500 nm. Perhaps the most important result in Fig. 3 is that the absorption and scattering spectra have essentially the same widths, which implies that the same mechanism for narrowing applies.

We now use the infinite lattice formula to evaluate the extinction cross section for one dimensional arrays of 50 nm particles. Figure 4(a) presents the results, and the retarded dipole sum S that is used in the evaluation of Eq. (5) is presented in the inset to the figure. In this case the plasmon peak intensities are higher and the widths narrower than the

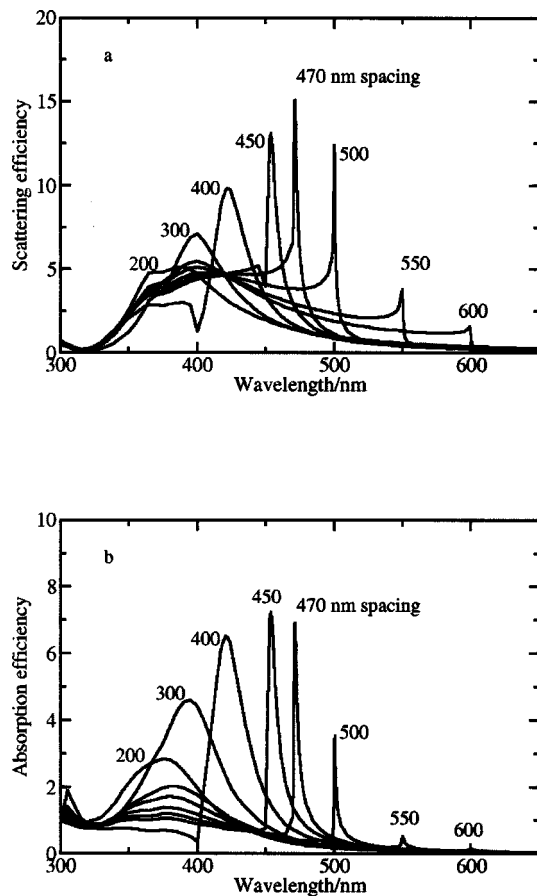


FIG. 3. Scattering and absorption spectra of a 400 particle one dimensional chain of 50 nm radius particles whose extinction spectrum is plotted in Fig. 1(a).

400 particle array results in Fig. 1(a) for a given spacing. For 500 nm spacing, the peak extinction efficiency is 27 and the plasmon width is 0.6 nm (3 meV) for the infinite array while the corresponding values for the 400 particle array are 16 and 1.5 nm (7 meV), respectively. For 600 nm spacing, the extinction efficiency rises to 42 and the width drops to the incredibly narrow value 0.0002 nm (7×10^{-4} meV). For 650 nm spacing the intensity falls to 15 and the width is still 0.0002 nm. We should also note that the plasmon wavelength is closer and closer in value to the interparticle spacing as the spacing gets larger. When the distance is 470 nm, the plasmon wavelength is 471.4 nm, so the difference between the plasmon wavelength and the spacing is 1.4 nm. At 500 nm spacing, the plasmon wavelength is 500.2 nm and the difference is reduced to 0.2 nm.

The plasmon resonance behavior in Fig. 4(a) can be understood based on Eq. (5) and the real and imaginary parts of S which are plotted in the inset to the figure. The inset shows that the real part of S has a very sharp peak when λ equals the spacing D , while the imaginary part of S shows a sudden drop, going through zero at $\lambda = D$. The sharp peak occurs when $\text{Im}(S)$ is most negative, corresponding to λ slightly greater than D . From Eq. (6), for a one dimensional chain and $\theta_{ij} = \pi/2$, the dipole sum is dominated by the term $\sum_{j \neq i} (k^2 e^{ikr_{ij}/r_{ij}})$. This sum can be done analytically, yielding an imaginary part $(2k^2/D)(\pi - \tau)$, where $\tau = 2\pi(D$

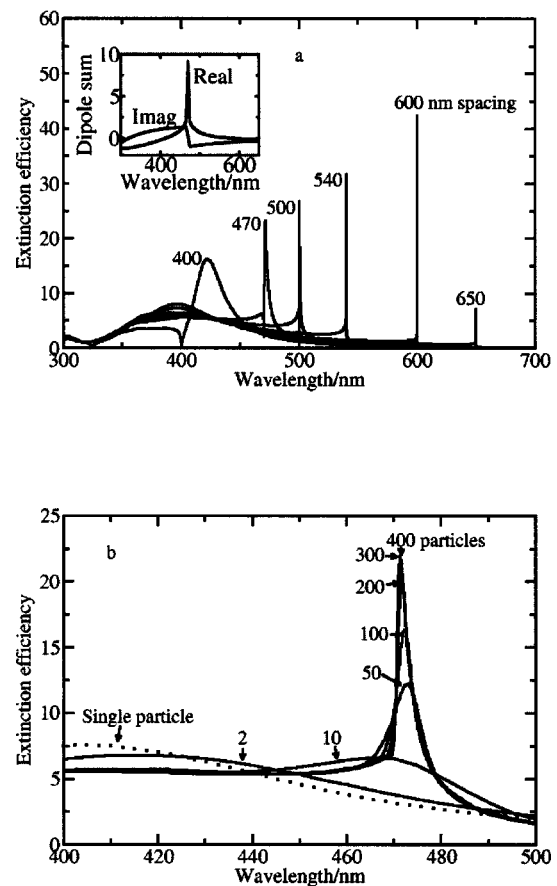


FIG. 4. (a) Extinction spectra of an infinite one dimensional chain of 50 nm silver nanoparticles. Inset shows the real and imaginary parts of the normalized dipole sum for a spacing of 470 nm. Both real and imaginary parts have been scaled by 0.001. (b) Extinction spectra of one dimensional chain of 50 nm particles for a spacing of 470 nm with chain size varying from 10 to 400 particles.

$-\lambda)/\lambda$ for $\lambda < D$ and $\tau = 2\pi D/\lambda$ for $\lambda > D$. Thus the imaginary part of the dipole sum becomes $\pm 8\pi^3/D^3$ on either side of the sudden drop at $\lambda = D$. Equation (7) then indicates that the width can go to zero provided that $\gamma \leq 8\pi^3 A/D^3$. For a sphere in the quasistatic limit, and using the Drude model for the dielectric constant, one can show that $A = \frac{1}{2}\omega_p r^3$, where the plasmon frequency ω_p is about 3.5 eV for Ag and r is the radius. Since D cannot be less than about 350 nm (as the plasmon resonances are all broad for $\lambda < 350$ nm due to interband effects), this puts a lower bound on the radius that produces zero width given by $r = (D/2\pi) \times (2\gamma/\omega_p)^{1/3}$. If we take γ to be 0.12 eV (which provides a reasonable fit to silver properties), the minimum radius is found to be 23 nm, in agreement with our numerical evaluation.

The results for 1D arrays having different numbers of particles, all with radius 50 nm and a spacing of 470 nm, are presented in Fig. 4(b). This shows that arrays with 10 particles give broad spectra, but 50 particles produce a width of about 10 nm and the width continuously narrows with further increases in array size. The extinction efficiency increases as the width decreases, varying from 12 for 50 particles to 20 for 200 particles. Note also that there is a slight blue-shift in the plasmon wavelength in going from 50 to 400 particles.

This shift arises because the imaginary part of S exhibits a sharper drop at $\lambda = D$ as particle number increases.

Using CD methods for finite and periodic lattices, we have studied the extinction spectra of one and two dimensional arrays of spherical silver nanoparticles. Narrow peaks whose widths a few nm are obtained, corresponding to energy widths of a few meV or less. We find that one dimensional chains for which polarization and wave vector are both perpendicular to the chain axis have the narrowest plasmon resonances. By changing the particle size and interparticle distance, we are able to obtain narrow peaks throughout the visible region. We find that the narrow peaks only appear in arrays with nanoparticle radii of 30 nm or greater. The narrow plasmon lineshapes can be produced for arrays of 50 particles, but the narrowest lines (nominally zero width in some cases) are for infinite chains.

The origin of the narrow peaks was examined using the infinite lattice model, and we find that for large enough particles the imaginary part of the retarded dipole sum can become sufficiently negative to cancel the single particle width. This occurs when the real part of the dipole sum is positive, so the plasmon peak is red-shifted from the isolated particle result. To achieve this cancellation it is essential for the wavelength to be slightly larger than the interparticle separation, as the detuned radiative dipolar interaction has a large negative imaginary part under these circumstances. Note, however, that there is always a broad "tail" to the lines we describe, which is an indication that the interference narrowing that we highlight here only operates over a small window of wavelengths and does not in the broader sense "quench" plasmon dephasing effects that are responsible for the intrinsic width of the plasmon.

The present results should be of significant importance to attempts to make plasmon-based chemical and biological sensors that use the change in the plasmon wavelength with analyte binding to determine concentration. In studies to be reported later²⁷ we find that although the plasmon wavelength shift with analyte binding is smaller for the 1D arrays than for isolated particles, the ratio of shift to width is larger by at least a factor of two, which means that the arrays will provide better sensitivity. We note that the structures needed for the present mechanism involve relatively large particles (>30 nm radius) and large spacings, both of which are amenable to preparation by a variety of lithographic methods. In addition, the same physical mechanism should work for par-

ticles of any shape, and for particles fabricated on a substrate.

We acknowledge support of the Nanoscale Science and Engineering Initiative of the National Science Foundation under NSF Award No. EEC-0118025. Any opinions, findings, and conclusions or recommendations expressed in this material are those of the author(s) and do not necessarily reflect those of the National Science Foundation. We also acknowledge AFOSR MURI Grant No. F49620-01-1-0381.

- ¹J. J. Storhoff, R. Elghanian, R. C. Mucic, C. A. Mirkin, and R. L. Letsinger, *J. Am. Chem. Soc.* **120**, 1959 (1998).
- ²B. H. Schneider, E. L. Dickinson, M. D. Vach, J. V. Hoijer, and L. V. Howard, *Biosens. Bioelectron.* **15**, 597 (2000).
- ³H.-L. Zhang, S. D. Evans, J. R. Henderson, R. E. Miles, and T.-H. Shen, *Nanotechnology* **13**, 439 (2002).
- ⁴E. Hutter, J. H. Fendler, and D. Roy, *J. Phys. Chem. B* **105**, 11159 (2001).
- ⁵Z. Gu, R. Horie, S. Kubo, Y. Yamada, A. Fujishima, and O. Sato, *Agnew. Chem.* **41**, 1153 (2002).
- ⁶N. Felidy, J. Aubard, G. Levi, J. R. Krenn, M. Salerno, G. Schider, B. Lamprecht, A. Leitner, and F. R. Aussenegg, *Phys. Rev. B* **65**, 075419/1 (2002).
- ⁷P. Royer, J. P. Goudonnet, R. J. Warmack, and T. L. Ferrell, *Phys. Rev. B* **35**, 3753 (1987).
- ⁸C. A. Foss, G. L. Hornyak, J. A. Stockert, and C. Martin, *J. Phys. Chem.* **98**, 2963 (1994).
- ⁹P. M. Tomchuk and B. P. Tomchuk, *J. Exp. Theor. Phys.* **85**, 360 (1997).
- ¹⁰H. Hovel, S. Fritz, A. Hilger, and U. Kreibig, *Phys. Rev. B* **48**, 18178 (1993).
- ¹¹U. Kreibig and M. Vollmer, *Optical Properties of Metal Clusters* (Springer-Verlag: New York, 1995), Vol. 25.
- ¹²M. Quinten and U. Kreibig, *Appl. Opt.* **32**, 6173 (1993).
- ¹³S. Malynych and G. Chumanov, *J. Am. Chem. Soc.* **125**, 2896 (2002).
- ¹⁴A. Taleb, C. Petit, and M. P. Pileni, *Phys. Rev. B* **102**, 2214 (1998).
- ¹⁵A. Taleb, V. Russier, A. County, and M. P. Pileni, *Phys. Rev. B* **59**, 13350 (1999).
- ¹⁶K. L. Kelly, E. Coronado, L. Zhao, and G. C. Schatz, *J. Phys. Chem. B* **107**, 668 (2003).
- ¹⁷L. Zhao, K. L. Kelly, and G. C. Schatz, *J. Phys. Chem. B* **107**, 7343 (2003).
- ¹⁸S. Zou, L. Zhao, and G. C. Schatz, *Proc. SPIE* **5221**, 174 (2003).
- ¹⁹S. Zou, L. Zhao, and G. C. Schatz (unpublished).
- ²⁰Y. W. C. Cao, R. C. Jin, and C. A. Mirkin, *Science* **297**, 1536 (2002).
- ²¹A. Haes and R. P. Van Duyne, *J. Am. Chem. Soc.* **124**, 10596 (2002).
- ²²C. L. Haynes, A. D. McFarland, L. Zhao, G. C. Schatz, R. P. Van Duyne, L. Gunnarsson, J. Prikulis, B. Kasemo, and M. Käll, *J. Phys. Chem. B* **107**, 7337 (2003).
- ²³V. A. Markel, *J. Mod. Opt.* **40**, 2281 (1993).
- ²⁴U. Laor and G. C. Schatz, *Chem. Phys. Lett.* **82**, 566 (1981).
- ²⁵E. D. Palik, *Handbook of Optical Constants of Solids* (Academic, New York, 1985).
- ²⁶A. A. Lazarides and G. C. Schatz, *J. Phys. Chem.* **104**, 460 (2000).
- ²⁷S. Zou and G. C. Schatz (unpublished).